Electropneumatic and Electrohydraulic Instruments: Modeling of Electrohydraulic and Electrohydrostatic Actuators

99.1 Introduction
99.2 Background
Actuator Modeling Requirements
99.3 Hydraulic Actuator Modeling
99.4 EHA Actuator Modeling
Motor • Pump and Fluid • Piston and Flight Control Surface • Quantitative Feedback Theory (QFT)
99.5 Actuator Compensator Design
99.6 Conclusion

M. Pachter and
C. H. Houpis
Air Force Institute of Technology

99.1 Introduction

In control systems, the output of the controller (also of the equalizer or compensator), which operates on the command (and feedback) input signals, is invariably sent to an actuator. The latter is a power element critically positioned at the plant input, and, to a large extent, determines the performance of the overall control system. Thus, the importance of the accurate modeling of the actuator element with respect to achieving and maintaining the desired control system performance over its operating range cannot be overemphasized. The impact of items such as the actuator phase lag characteristics, parameter variations and aging, sensor noise, and operating scenario (e.g., in a flight control context it is referred to as *flight conditions*) should be explicitly considered in a control system design process. To achieve a robust control system, where these items are taken into account, requires a good understanding and an accurate model of the actuation element. This chapter discusses the actuator modeling process.

99.2 Background

Power-to-weight considerations have driven actuator design to pneumatic, hydraulic, electrohydraulic, and recently, in flight control applications, electrohydrostatic configurations. In this chapter the point of view

is taken that the actuator element constitutes a feedback control system in its own right. Thus, the actuator comprises of an "amplifier" element (the servo valve), a power element (the "ram"), an actuator displacement sensor, and a controller about which more will be said in the sequel. Furthermore, it is important that the actuator subsystem be considered in the context of the complete control system, e.g., a flight control system. This point of view is promulgated throughout this chapter. First, a relatively simple hydraulic actuator is considered. The focus then shifts to the modern electrohydrostatic actuator (EHA) technology which, in the flight control application, offers a high degree of combat survivability and easier maintainability since its components are collocated with the actuator. Since the EHA does not require long hydraulic lines, required maintenance time and equipment can be reduced. This also substantially reduces the profile exposed to hostile fire. In addition, actuator failures due to various causes and/or aging need to be taken into account in designing the overall control system. The design of a robust control system, utilizing an actuator, requires an accurate actuator model in order to satisfy the system performance specifications. The EHA and its flight control application are used as the "vehicle" for presenting the actuator modeling process.

Actuator Modeling Requirements

When an actuator needs to be replaced in a control system, for reasons cited previously, by one "off the shelf," the robustness of the overall control system must be unaffected by this replacement unit. Thus, the actuator design process entails

1. The derivation of an accurate mathematical model for the actuator.
2. Sensitivity analyses on the actuator control systems. This should include sensitivity to variations in load, component efficiencies, physical plant parameters, and actuator sensor noise.
3. The identification of a reasonable set of plant variations for the actuator, based on the sensitivity analysis, which is required for designing a robust actuator control system that will meet the specifications in the presence of predicted variations.

99.3 Hydraulic Actuator Modeling

The modeling of a purely hydraulic actuator employed in an irreversible flight control system is presented first. Based upon the notation shown in Fig. 99.1 the following relationships are obtained:

$$x_1 = \delta_{e_c} a \tag{99.1a}$$

$$\frac{x_v - x_f}{b+c} = \frac{x_v - x_l}{c} \tag{99.1b}$$

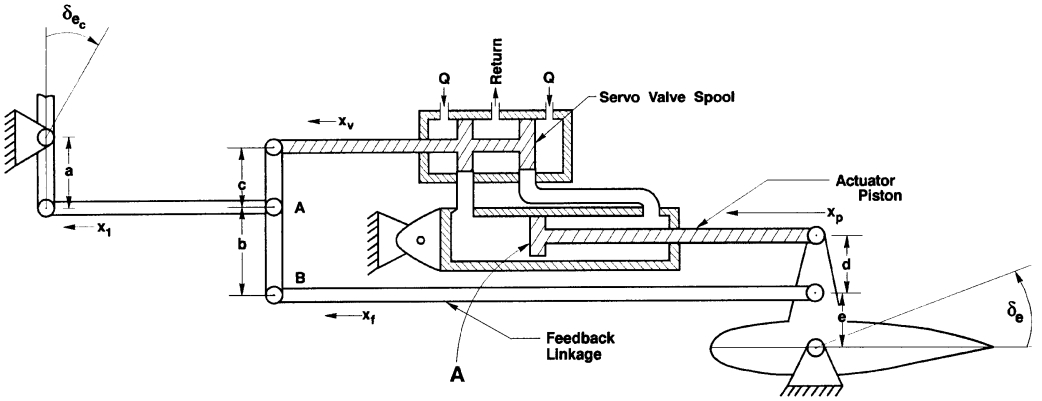

FIGURE 99.1 Irreversible control system.

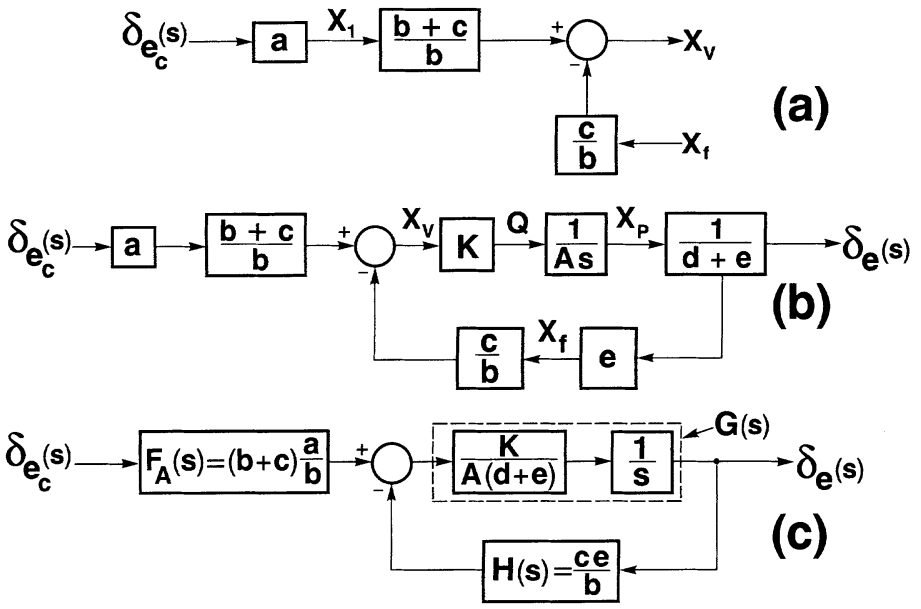

FIGURE 99.2 (a) Actuator block diagram; (b) block diagram of actuator feedback control system; (c) simplified block diagram.

which yield

$$x_v b + x_f c = x_1(b + c) \tag{99.2}$$

From these equations Fig. 99.2a is obtained. Next, the relationships

$$\frac{dx_p}{dt} = \frac{Q}{A}, \quad Q = Kx_v, \quad \delta_e = \frac{x_p}{d+e}, \quad x_f = e\delta_e \tag{99.3}$$

are utilized to yield the block diagram of a typical feedback control system (shown in Fig. 99.2b) which represents the irreversible hydraulic actuator under consideration. This block diagram is simplified to the one shown in Fig. 99.2c, which yields the first-order transfer function of the actuator:

$$G(s) = \frac{\delta_e(s)}{\delta_{e_c}(s)} = \frac{K}{\tau s + 1} \tag{99.4}$$

where the gain $K = [a(b + c)]/ce$, the time constant $\tau = [Ab(d + e)]/cKe$ of the actuator, and $0.025 < \tau < 0.1$ s. For a step input command, a typical actuator time response is shown in Fig. 99.3.

More-detailed dynamic modeling of the valve leads to higher-order hydraulic actuator models. For example, the transfer function of the currently used actuator of the F-16 aircraft is of fourth order [1] and its frequency response is compared with its first-order approximation in Fig. 99.4. It is indeed important to use the full-blown high-order actuator dynamic model in robust control system design. As Fig. 99.4 shows, the simplified first-order model fits well the high-order model in the low-frequency range. Unfortunately, a significant phase angle difference exists at the higher frequencies where the actuator will be operating, for the higher frequencies are within the bandwidth of modern robust ("high gain") control system compensators.

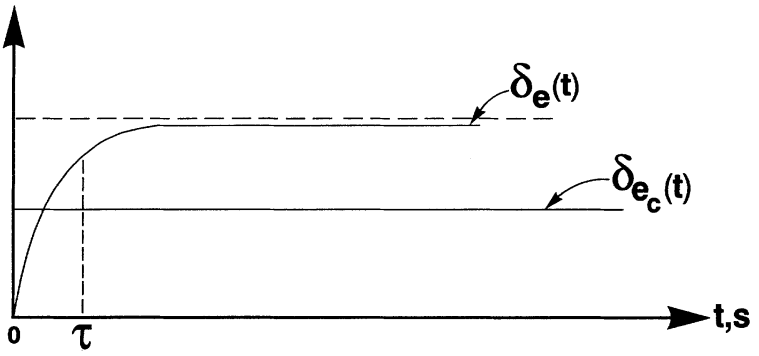

FIGURE 99.3 Time response of an actuator.

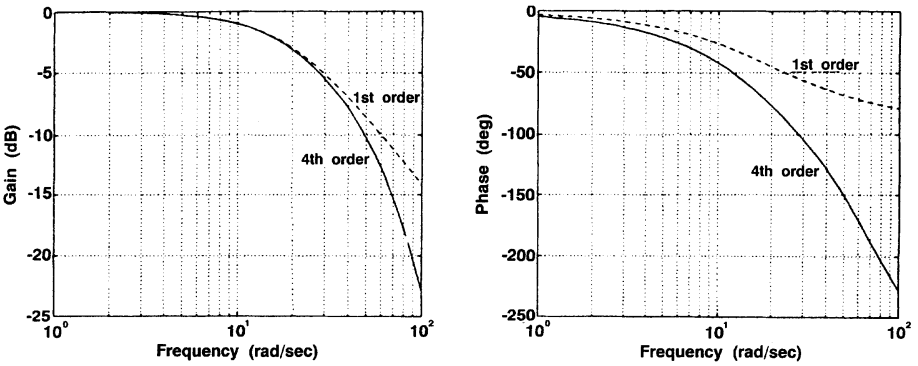

FIGURE 99.4 Comparison of first- and fourth-order actuator models.

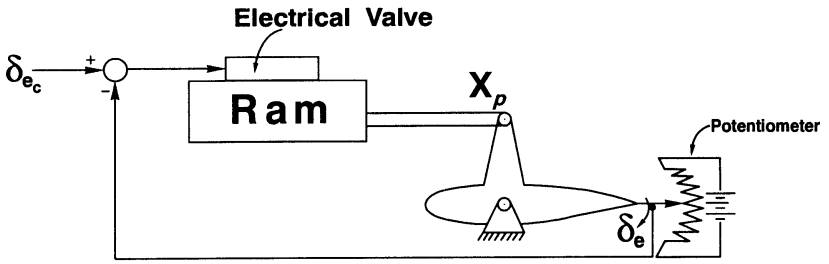

FIGURE 99.5 Electrohydraulic actuator.

The next step in the actuator state of development is then an electronic "fly-by-wire" mechanization of the feedback loop. This is shown in Fig. 99.5 where an actuator is shown that employs an electric (solenoid-controlled) valve, a potentiometer to measure the control surface deflection (actuator displacement), and where the power element of the actuator, the RAM, is an hydraulic cylinder.

99.4 EHA Actuator Modeling

The novel EHA actuator (see, e.g., Reference 2) offers a high degree of maintainability and survivability because all the actuator elements are collocated and a central hydraulic pump with the attendant high-pressure hydraulic plumbing is not needed. The modeling of the modules of the EHA is outlined first.

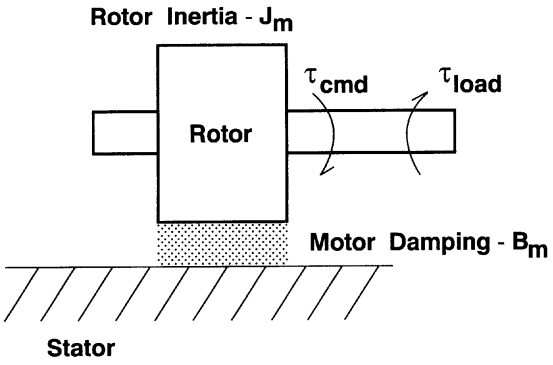

FIGURE 99.6 Motor model.

Motor

Electric motors with the rotor moment of inertia J_m and electromechanical damping B_m (see Fig. 99.6), are subject to variations in output torque and subsequent fluctuations in rotor speed ω_m. Since the torque due to the load counteracts the torque generated by the motor, perturbation may also be caused by variations of the load torque. This relationship is expressed as

$$\tau_e(s) = \tau_{cmd}(s) - \tau_{load}(s) \tag{99.5}$$

where τ_{load} is the load torque due to the differential pressure of the fluid in the pump. This results in a first-order transfer function

$$\frac{\Omega_m(s)}{\tau_e(s)} = \frac{1}{J_m s + b_m} \tag{99.6}$$

Pump and Fluid

Electric motors have a limited torque-to-mass ratio, due to the finite and limited magnetic flux density that can be generated [3]. High-pressure hydraulic systems, with the system pressure of 2000 to 5000 psi, can generate high forces resulting in more compact and higher torque-to-mass ratios than electric motors. Generally, high-pressure hydraulic systems are stiffer against the load than electric motors. Hence, the EHA utilizes a dc motor to pump high-pressure fluid into the piston chamber. The dc motor internal to the EHA converts the electric power into mechanical power. It is the pump that converts this mechanical power into hydraulic power. The hydraulic power, acting against the piston, is converted to mechanical power capable of moving the load, e.g., large flight control surfaces.

The flow rate Q_m generated by the pump is proportional to the motor speed, i.e.,

$$Q_m(s) = \frac{D_m}{2\pi}\Omega_m(s) \tag{99.7}$$

where D_m represents the pump displacement constant. The flow rate of the hydraulic fluid is primarily dependent on two factors: change in chamber volume and change in pressure due to the compressibility of the fluid effect [4]. The chamber volume changes as the piston moves through the chamber at speed dx_p/dt. The flow rate due to the changes in chamber volume is then expressed as $\pm A dx_p/dt$. Secondary fluid dynamic effects include fluid compressibility, internal leakage flow, and external leakage flow. These secondary effects are modeled by a first-order equation as follows:

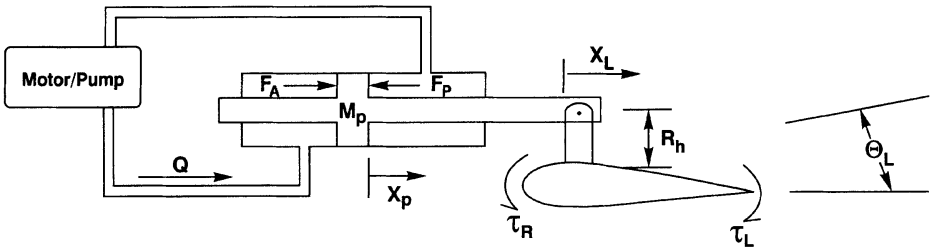

FIGURE 99.7 Simplified actuator control (not drawn to scale).

$$\delta Q(s) = Q_m(s) - AsX_p = \left[K_s s + C_t\right]P(s) \tag{99.8}$$

which results in the transfer function

$$\frac{P(s)}{\delta Q(s)} = \frac{1}{K_s s + C_l} \tag{99.9}$$

Piston and Flight Control Surface

Piston and Flight Control Surface Fundamentals

The pressure developed by the pump and fluid acts on the piston surface (see Fig. 99.7), causing the RAM to extend or retract. This force then generates a torque through a hinge to deflect the control surface. This torque has to overcome two load components: control surface inertia and aerodynamic loads. The control surface inertia is primarily due to the fact that the control surface has certain size and mass. The aerodynamic load only occurs in flight, when the air pressure over the control surface applies aerodynamic forces to it. The aerodynamic load is determined by three factors: the surface area of the flight control surface, aerodynamic loading which varies with altitude and airspeed, and the relative angle of the surface to the wind. The surface angle to the wind depends on the angle of surface deflection and on the angle of attack of the aircraft.

Piston and Flight Control Surface Dynamics

Flexible Hinge Joint Model

The magnitude of F_A acting on the piston is equal to $\wp A$, where $\wp$ is the differential pressure developed by the pump and fluid and A is the surface area of the piston. Thus, the force created by the pump and fluid can be expressed as

$$F_A = \wp A \tag{99.10}$$

The piston dynamics, with the piston mass M_p and piston damping B_p, can be described by the second-order model:

$$F_A - F_P = \left[M_P s^2 + B_P s\right]X_P \tag{99.11}$$

The resulting torque acting on the flight control surface due to this force imbalance can be described by

$$\tau_R = \frac{K_h}{R_h}\left(X_P - X_L\right) \tag{99.12}$$

where K_h is the hinge stiffness constant and R_h is the hinge length. The stabilator inertia acts against the torque generated by the actuator, such that

$$\tau_R - \tau_L = \left[J_L s^2 + B_L s\right]\theta_L \tag{99.13}$$

where τ_L is the torque created by the aerodynamic load and stabilator inertia. The variables J_L and B_L represent the mass properties of the flight control surface.

Stiff Hinge Joint Model

Equations 99.11 through 99.13 represent a rather complex model of load dynamics. The complexity of the model can be reduced if the linkage between the actuator and flight control surface is considered rigid. This is a valid assumption, since the natural frequency of the hinge for a well-designed actuation system is much greater than the actuator bandwidth of concern. Hence, the piston and load dynamics are still expressed as

$$F_A - F_P = \left[M_P s^2 + B_P s\right]X_P \tag{99.14}$$

and

$$\tau_R - \tau_L = \left[J_L s^2 + B_L s\right]\theta_L \tag{99.15}$$

Dividing Eq. 99.15 by R_h yields

$$F_R - \frac{\tau_L}{R_h} = \left[\frac{J_L s^2 + B_L s}{R_h}\right]\theta_L \tag{99.16}$$

Assuming rigidity of the hinge assembly, $F_R \approx F_P$. Hence, adding Eqs. 99.14 and 99.16 results in

$$F_A - \frac{\tau_L}{R_h} = \left[M_P s^2 + B_P s\right]X_P + \left[\frac{J_L s^2 + B_L s}{R_h}\right]\theta_L \tag{99.17}$$

where τ_L is defined as

$$\tau_L = \left(\text{Load}_{\text{aero}}\right)\theta_L \tag{99.18}$$

Since rigidity implies that $X_p = X_L$ and $\theta_L = X_p/R_h$, Eq. 99.17 is further reduced to

$$F_e = F_A - \frac{\tau_L}{R_h} = \left[\left(M_P + \frac{J_L}{R_h^2}\right)s^2 + \left(B_P \frac{B_L}{R_h^2}\right)s\right]X_P \tag{99.19}$$

or expressed in a transfer function form:

$$\frac{X_P(s)}{F_e(s)} = \frac{1}{s\left[\left(M_P + \frac{J_L}{R_h^2}\right)s + \left(B_P \frac{B_L}{R_h^2}\right)\right]} \tag{99.20}$$

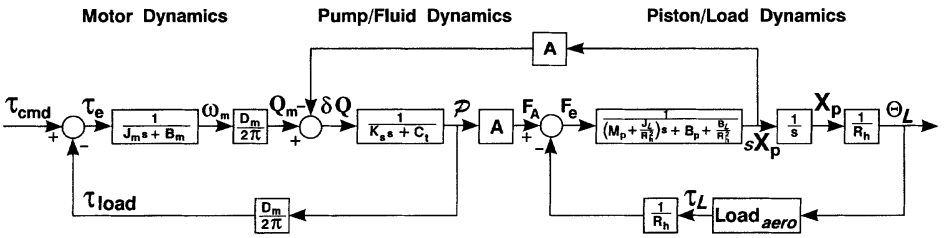

FIGURE 99.8 Bare EHA block diagram.

Equation 99.20 represents a simplified model of the load dynamics. A complete simplified design model of the bare EHA, without the controller, is shown in Fig. 99.8 using the individual component models.

Hinge Moments

The aerodynamic loads mentioned previously describe the torque opposing the piston motion. Thus, load generated by the flow of air above and below the flight control surface applies a torque to the hinge assembly, which in turn adds backpressure to the piston. The hinge moment is modeled as follows:

$$\tau_L = \bar{q} S_t R_h \left(Ch_\alpha \frac{\alpha(s)}{\theta_L(s)} + Ch_\delta \right) \theta_L \tag{99.21}$$

where S_t denotes the surface area of the control surface, $\bar{q}$ denotes the dynamic pressure, Ch_α and Ch_δ denote the hinge moment coefficients of the control surface with respect to angle of attack and surface deflection δ. The aerodynamic load dynamic pressure $\bar{q}$ is a function of airspeed U_0 and air density [2] ρ, as expressed by

$$\bar{q} = \frac{1}{2} \rho U_0^2 \tag{99.22}$$

The air density in a standard atmosphere drops exponentially with increasing altitude. The dynamic pressure $\bar{q}$ increases as the Mach number gets higher and altitude decreases. The hinge moment for modern fighters with all movable tails, where $Ch_\alpha \approx Ch_\delta$, is modeled by

$$\tau_L = \bar{q} S_t R_h Ch_\delta \left(\frac{\alpha(s)}{\theta_L(s)} + 1 \right) \theta_L \tag{99.23}$$

Aircraft Short Period Approximation

If the aircraft forward speed is assumed constant (i.e., the speed perturbations $u \approx 0$), the X force equation can be neglected since it does not significantly contribute to the short-period oscillation [5]. Thereby, the short-period approximation of the longitudinal channel of the aircraft which is relevant to the actuator dynamics is extracted and is written as

$$\begin{bmatrix} \dot{\alpha} \\ \dot{q} \end{bmatrix} = \begin{bmatrix} z_\alpha & z_q \\ m_\alpha & m_q \end{bmatrix} \begin{bmatrix} \alpha \\ q \end{bmatrix} + \begin{bmatrix} z_\delta \\ M_\delta \end{bmatrix} \begin{bmatrix} \delta_e \end{bmatrix} \tag{99.24}$$

This yields a second-order minimum-phase transfer function of the form:

$$\frac{\alpha(s)}{\delta(s)} = \frac{-K(s+a)}{(s+b)(s+c)} \tag{99.25}$$

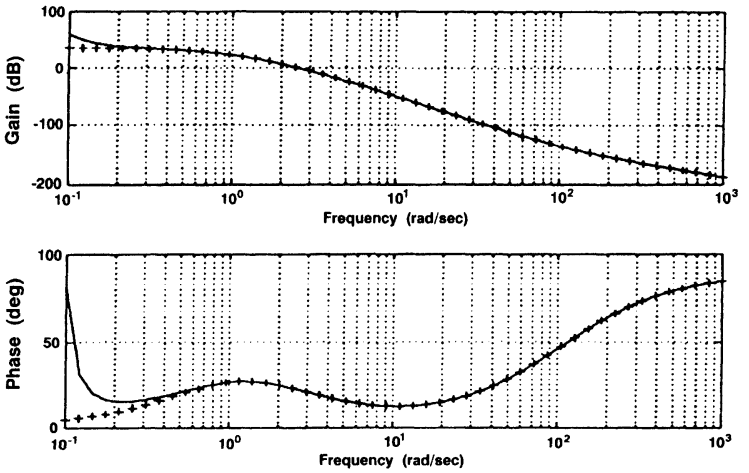

FIGURE 99.9 Comparison of full and short period approximation for longitudinal equations of motions.

For the frequency of interest, the short-period approximation closely resembles the full state model. As seen in Fig. 99.9, where the solid lines represent the full state model frequency response of the vehicle and + lines represent the short-period model frequency response of the vehicle, phase and attenuation characteristics are closely matched at high frequency. The approximation, as seen in the figure, is not valid for frequencies below 0.5 rad/s due to the effects from the slow longitudinal mode, which is referred to as the phugoid.

Quantitative Feedback Theory (QFT)

Robust QFT [3,6] compensators are ideal for obtaining the desired response from an actuator. The term *robust* in control theory implies that a system under control, in this case the actuator, remains stable throughout its operating envelope, rejects disturbances, and results in minimum degradation in the performance specifications. A QFT designed feedback system, which uses output feedback, assures that the output tracks the input values despite parametric uncertainties or disturbances. The output of a unity-gain feedback system with uncertain plant models can vary depending on the plant conditions; however, the output of a robust QFT feedback control system with uncertain plant models will not vary much. The unity-gain system, however, cannot control the tracking response, which necessitates the inclusion of a prefilter.

Plant (specifically, actuator) uncertainties may be caused by manufacturing tolerances. For example, a component *A* is specified to be 10 ± 0.1 mm long. In a large production run, the length of component *A* may be anywhere between 9.9 and 10.1 mm. This tolerance range may be substantial enough to produce noticeable variations in the plant model. Plant uncertainties may also be caused by the environment, specifically the system (actuator) operating conditions. For example, the parameters of an aircraft model display large variations depending on altitude and airspeed. Finally, the performance of various components decay over time, introducing an additional element of uncertainty.

The QFT design paradigm accounts for the plant variations in the design procedure. It is a linear design technique for designing a linear robust controller for linear or nonlinear control systems [3,6] — in this case the actuator control system. As long as all the QFT design requirements are met, the output responses are guaranteed to conform to the specification boundaries. The initial step in the design process is to establish the upper and lower performance tracking boundaries. The maximum allowable disturbance is used to determine the disturbance boundary. The phase margin angle, gain margin, or maximum peak value is used to establish the stability boundary. These combined boundaries establish the limitation of the system performance. The next step is to analyze the system to determine the parameters that will

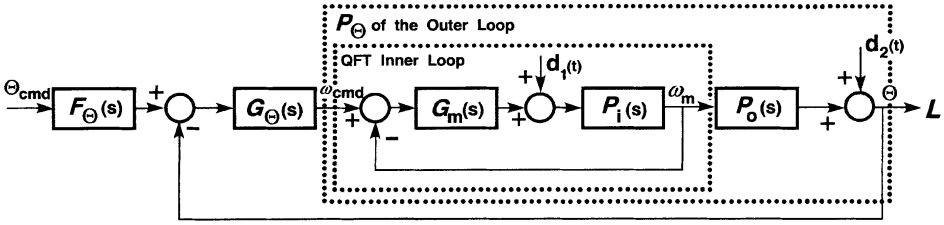

FIGURE 99.10 Two feedback loops in QFT two degrees of freedom structure.

cause noticeable variations to the plant. The system, often modeled only as a single plant transfer function in other design methods, is now modeled more completely as a *set* of plant transfer functions. The variations now form a closed region in the Nichols magnitude and phase chart, called the template; larger template sizes indicate a higher degree of plant uncertainty. Templates at different frequencies differ in size and shape.

A most important aspect of modeling is the thorough analysis of the bare actuator plant, in order to find the sources of plant variation. For an aircraft application the three largest sources of variations are the fluctuations in aerodynamic load on the flight control surfaces, motor torque, and hydraulic pump fluid pressure.

99.5 Actuator Compensator Design

QFT compensators, which are designed in the frequency domain, are ideally suited for the actuator control system. The QFT compensator processes its inputs, which are the commanded actuator displacement and the measured current actuator position, and generates a commanded signal to, e.g., the solenoid valve in a hydraulic actuator, or a current for the electric dc motor in the EHA actuator. In order to proceed with the actuator QFT compensator design, the block diagram as shown in Fig. 99.7 is transformed to the standard inner and outer QFT loop structures shown in Fig. 99.10 [2,3,6]. For this design problem the external disturbance $d_2(t)$ can be ignored, i.e., $d_2(t) = 0$, whereas the $d_1(t)$ disturbance models a possible measurement bias. The inner loop controls the angular rate of the motor while the outer loop controls the surface deflection. Since tracking in the inner loop is less important, for its function is to reduce the uncertainty level of the outer loop, the inner loop prefilter can be set to unity and the tracking performance enforcement is relegated to the prefilter F_θ of the outer loop.

99.6 Conclusion

The modeling of a hierarchy of hydraulic actuators has been presented. The modeling of modern EHAs is emphasized and dynamic models of its subcomponents are carefully developed. A systems approach to actuator modeling and design is taken and the feedback structure is highlighted. In this chapter it is stressed that, because of the complex feedback interactions at work, proper actuator modeling requires consideration of the latter in the full context of the control system in which it is to be employed. Thus, in this presentation the aerospace application is considered. At the same time the actuator is being viewed not as a component of a control system, but as a control system in its own right. Hence, it is shown that simple mechanical feedback linkages which fulfilled the role of a controlling element for the actuator can be replaced by a more flexible, high-performance, robust, full-blown electronic actuator compensator. Concerning electropneumatic instruments and sensors, these are critical elements in systems where the flow of liquids and/or gases is being controlled, e.g., in the chemical industries. In aerospace, electropneumatic sensors are used to measure airspeed, altitude, and the angle of attack and sideslip angles of the aircraft; these functions are collocated in the air data computer (ADC). Currently, modern sensors use feedback action for accuracy enhancement, and, as such, the design of modern electropneumatic

instruments and sensors is conceptually similar to the design of EHAs. Detailed information on actuators and sensors may be found in References 4 and 7.

Nomenclature

A	ram cross section area
a,b,c,d,e,R_h	length of linkages
x,X	displacement
J	moment of inertia; o, ovin
K	gain
Q	flow rate
s	Laplace variable
D_m	pump displacement constant
F	force
M_p	mass of piston
B_p	piston damping
K_h	hinge stiffness constant
$\bar{q}$	dynamic pressure
S_t	aerodynamic surface area
C_h	hinge moment coefficient
U,u	airspeed
q	pitch rate
M,z,m	aerodynamic stability derivatives
P	pressure
δ	deflection angle
τ	torque
Ω, ω	rotor speed
P	differential pressure developed by the pump
θ	deflection angle
α	angle of attack of aircraft
ρ	air density

References

1. O.R. Reynolds, M. Pachter, and C.H. Houpis, Full Envelope Flight Control System Design Using Quantitative Feedback Theory, *AIAA J. Guidance Control Dyn.*, 19, 1023–1029, 1996.
2. K.H. Kang, Electro-Hydrostatic Actuator Controller Design Using Quantitative Feedback Theory, MS thesis, Graduate School of Engineering, Air Force Institute of Technology, Wright-Patterson AFB, OH, December 1994, AFIT/GE/ENG/94D-18.
3. C.H. Houpis, M. Pachter, S. Rasmussen, and R. Sating, Quantitative Feedback Theory for the Engineer, Wright Laboratory Technical Report, WL-TR-95-3061, Wright Laboratory, Wright-Patterson AFB, OH, June 1995. (Available from the National Technical Information Service, 5285 Port Royal Road, Springfield, VA 22151, document number AD-A297574.)
4. C.W. de Silva, *Control Sensors and Actuators*, Englewood Cliffs, NJ: Prentice-Hall, 1989.
5. J.H. Blakelock, *Automatic Control of Aircraft and Missiles*, New York: John Wiley & Sons, 1991.
6. J.J. D'Azzo and C.H. Houpis, *Linear Control System Analysis and Design — Conventional and Modern*, 4th ed., New York: McGraw-Hill, 1988.
7. E.H.J. Pallet and S. Coyle, *Automatic Flight Control*, Oxford, U.K., Blackwell, 1993.